Available online at www.sciencedirect.com
SCIENCE DIRECT®
Electrochimica Acta 50 (2005) 5229–5236
ELECTROCHIMICA Acta
www.elsevier.com/locate/electacta

Bubble visualization and electrolyte dependency of dissolving hydrogen in electrolyzed water using Solid-Polymer-Electrolyte

Yoshinori Tanaka [a,c,*], Kenji Kikuchi [b], Yasuhiro Saihara [a], Zempachi Ogumi [c]

[a] *Matsushita Electric Works Ltd., Research & Development Center, Home Appliances Co., Kadoma, Osaka 571-8686, Japan*
[b] *Department of Materials Science, University of Shiga Prefecture, 2500 Hassaka, Hikone, Shiga 522-8533, Japan*
[c] *Department of Energy and Hydrocarbon Chemistry, Graduate School of Engineering, Kyoto University, Kyoto 615-8510, Japan*

Received 19 October 2004; received in revised form 11 January 2005; accepted 11 January 2005

Abstract

Solid-polymer-electrolyte electrolysis was performed in electrolyte solutions of different concentrations. The higher the electrolyte concentration, the higher the concentration of dissolved hydrogen as H_2 molecule. The concentration of dissolved hydrogen was high in the high electrolyte solutions only when current density was high. In an effort to clarify this finding, the electrolytic generated hydrogen bubble was visualized using a high speed camera. Numerous bubbles were formed under high current density, therefore, the degree of bubble coalescence increased. The bubble coalescence, however, was inhibited by addition of electrolytes. In the electrolyte solution, the hydrogen bubbles maintained the released bubble size. The high concentration of dissolved hydrogen was attributable to the bubble coalescence inhibited by the electrolyte.

Keywords: Bubble visualization; Hydrogen dissolution; Electrolyte solution; Water electrolysis; Solid-polymer-electrolyte

1. Introduction

A catholyte obtained from tap water electrolysis is called "alkali-ion-water" in Japan. Alkali-ion-water contains dissolved hydrogen and is potable. The dissolved H_2 molecule is thought to be beneficial to one's health [1–3]. Further, water electrolysis is a convenient means to dissolve the hydrogen in the water because hydrogen is supersaturated in the vicinity of the electrode [4] and it is a very simple means to produce fine bubbles [5,6]. However, the electrolyzed water in the catholyte, contains hydrogen with an alkaline pH.

Tashiro et al. reported, based on clinical test results, that alkali-ion-water at a pH higher than 10 may cause an increase in potassium ions in the blood, in rare cases [1]. Therefore, the pH of "alkali-ion-water" has been regulated to remain below 9.8. Thus, it is important to produce "alkali-ion-water" with a high concentration of dissolved hydrogen, while maintaining a pH below 9.8. With conventional electrolysis, it is difficult to enhance the hydrogen content of "alkali-ion-water" to the saturation level without an increase in the pH to values over 10.

In water electrolysis using an SPE electrolyzer, hydrogen is generated efficiently for the current and the cell potential is significantly lower than that when using the plate electrodes of an alkali-ion-water electrolyzer [7,8]. Further, hydrogen is generated at a contact point between the SPE and the plated Pt electrode, and it is released from the crack of the plated electrode to the water outside the electrode. On the cathode, the hydrogen is generated from the hydrogen ions and, therefore, it is easy to enhance the hydrogen content of the catholyte up to saturation without an increase pH over 10 using a SPE electrolyzer.

The hydrogen released from the plated Pt electrode forms fine bubbles partially dissolved into the water as H_2 molecule.

* Corresponding author.

0013-4686/$ – see front matter © 2005 Elsevier Ltd. All rights reserved.
doi:10.1016/j.electacta.2005.01.062

The hydrogen bubble is known to have a tiny amount of electric charge. The electric charge is thought to affect the stability and the coalescence of the bubbles, thereby affecting the dissolution of the bubble.

A number of researchers have measured the zeta potential of the bubble [9–14]. Brandon et al. reported the hydrogen bubble is negatively charged at pH > 3. Further, he reported that the bubble rise rate was decreased upon addition of the electrolyte [13]. Yang et al. reported that the variation of the bubble zeta potential with pH depended on not only the electrolyte concentration but also the kind of metal ions [14].

Additionally, the small bubbles coalesce into large bubbles [15–21]. Zarra reported that the higher the electrolyte concentration, the lower the rate of bubble coalescence [15]. Bubble rise velocity is known to decrease with increasing electrolyte concentration. Craig et al. reported the effect of electrolytes on bubble coalescence [16]. They observed that some electrolytes have no effect on bubble coalescence. In addition, a property (α or β) was assigned to each anion and cation. The combinations of (αα) or (ββ) inhibit coalescence, whereas (αβ) or (βα) have no effect. These observations were explained by the local influence of ions on the water structure, possibly in a way related to hydrophobic interaction.

Recently, sub-micrometer bubbles are thought to be present in the water. These nanobubbles, or tiny gas bubbles that have been found on some surfaces in liquids, were proposed by Tyrrell and Attard [23]. An image of these nanobubbles was obtained using a scanning probe microscope in the tapping mode. The nanobubbles are from 10 to 100 nm in diameter and their lifetime is on the order of hours, at the least. Kim et al. measured the zeta potential of nanobubbles generated using ultrasonics [24].

Kikuchi et al. elucidated the existence of hydrogen particles as a colloid (below about 600 nm) in electrolyzed water using the DLS method [6]. The diameter of hydrogen particles was found to decrease with an increase in the sodium chloride concentration.

An SPE electrolyzer was used to measure the ratio of the dissolved hydrogen content to the amount of hydrogen produced and found that it is affected by the current density and the rate of the supplied water [25,26]. In the case of a high bubble population, the bubbles were found to coalesce with each other forming a large bubble. The rise velocity of the large bubble was significantly faster than that of the small bubble, and the inner pressure of the large bubble was significantly lower than that of the small bubble. The rapid rise velocity and the low inner pressure result in the low dissolving efficiency of the hydrogen from the bubble. The coalescence of the hydrogen bubbles affects the hydrogen concentration. The objective of this study was to clarify the effect of electrolytes on the concentration of dissolved hydrogen in the catholyte under the same current density and the same rate of the supplied water using an SPE electrolyzer.

2. Experimental

Electrolysis cells used in the present investigation are shown in Fig. 1 (visualization of bubble generation and contraction), Fig. 2 (visualization of bubble contraction) and Fig. 3 (electrolyte dependence).

2.1. Generation of hydrogen bubbles

In order to visualize the bubble generation, one side of a Nafion® (N-117, DuPont) membrane was plated using a chemical platinum-plating method [8]. The protons in Nafion were exchanged to form Pt complex ions. The Pt complex ion was reduced to Pt using $NaBH_4$ on the surface of the Nafion membrane. The plated Pt electrode was 0.5 μm thick. The electrolysis cell is shown in Fig. 1. The Nafion membrane plated with platinum (geometrical area; 20 mm × 8 mm) was set as a diaphragm separating two cathode chambers, I and II. The plated side of the Nafion membrane was maintained facing cathode chamber II. Another Nafion membrane was set as a diaphragm separating cathode chamber I and the anode chamber. The plated platinum electrodes were held down by current feeders, consisting of titanium and electroplated with platinum. A Pt plate was used as the anode. A 0.33 mol dm^{-3} Na_2SO_4 solution was stored in the chambers. In order to distinguish the bubbles adhering to the Pt and the Nafion, cathode chamber II was either filled or emptied. An X-ray Imaging camera (C4880-50-24A, Hamamatsu Pho-

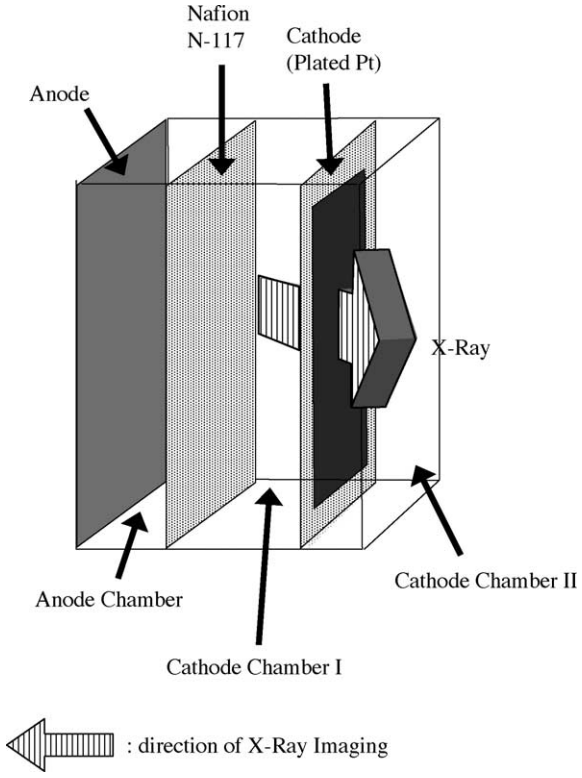

Fig. 1. Schematic of electrolytic cell used for visualization of bubble generation and bubble contraction by X-ray imaging.

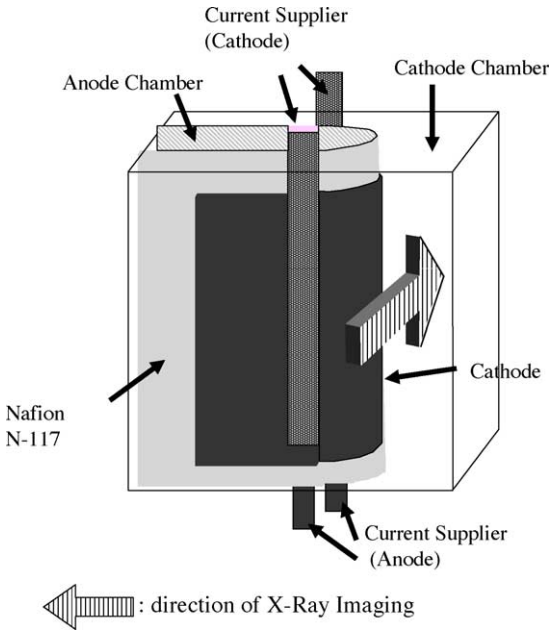

Fig. 2. Schematic of electrolytic cell used to visualize bubble contraction by X-ray imaging.

tonics) (X-rays (30 keV)) was used to visualize the hydrogen bubbles using the BL19B2 of SPring-8 [28,29]. Hydrogen bubbles were captured by X-ray transmitting the Nafion and thin plated Pt electrodes. Electrolysis was performed under a constant current at room temperature. The 20 mA current was controlled using a potentio-galvanostat (HA-301, Hokuto Denko Corp.).

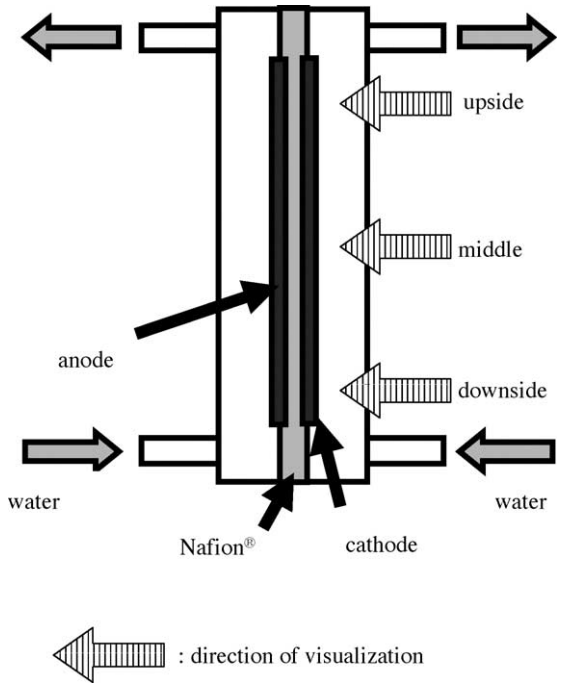

Fig. 3. Schematic of electrolytic cell used to measuring hydrogen concentration and bubble visualization using high speed digital imaging camera.

2.2. Contraction of hydrogen bubbles

In order to visualize the bubble contraction, the single-sided Nafion–Pt electrode complex and the double-sided Nafion–Pt electrode complex were used to distinguish the effect of the distance between the cathode and anode. Both sides of the Nafion membrane were plated with the platinum (50 mm × 50 mm) bent into a U-shape, as shown in Fig. 2. The membrane was set as a diaphragm separating the outer cathode chamber and the inner anode chamber. The plated platinum electrodes were sandwiched by two pairs of current feeders. A 0.33 mol dm^{-3} Na_2SO_4 solution was stored in the chambers of two types of Nafion–Pt electrode complexes. The 40 mA current was controlled using a potentio-galvanostat for 5 min. After turning off the current, the hydrogen bubbles were visualized using an X-ray imaging camera. In the single-sided Nafion–Pt electrode complex, hydrogen bubbles adhering to Pt were captured by X-ray transmission of the Nafion and thin Pt electrode. In the double-sided Pt–Nafion–Pt electrode complex, hydrogen bubbles adhering to Pt were captured grazing the curve of U-shape with an X-ray.

2.3. Effect of electrolyte and coalescence of hydrogen bubbles

Another Nafion membrane was plated on both sides for other measurements. The Nafion membrane plated with the platinum (geometrical area; 106 mm × 30 mm) was set as a diaphragm separating the cathode and anode chamber. The electrolysis cell is shown in Fig. 3. The plated platinum electrodes were sandwiched by two current feeders.

Electrolyte dependence and concentration dependence were measured in distilled water and electrolyte solution. The electrolyte solutions consisted of NaCl, KCl and LiCl solutions of 0.01 and 0.1 and 1 mol dm^{-3} concentrations, and Na_2SO_4, K_2SO_4 and Li_2SO_4 solutions of 0.01, 0.1 mol dm^{-3} concentrations. The electrolyte solution was supplied to the cell by pumping at a constant mass flow rate of 0.1 dm^3 s^{-1}. Electrolysis was performed under a constant current and at room temperature. The current density ranged from 0.3 to 3.0 A dm^{-2} and was controlled using the potentio-galvanostat. The electrolyzed water from the cathode chamber was introduced into the beaker. The dissolved hydrogen, H_2 molecule, was measured using a dissolved hydrogen meter (DH-meter, DH-35A, DKK-TOA Corporation).

A high speed digital imaging camera (V7.0, Vision Research Phantom) was used to visualize the rising bubbles in distilled water and the electrolyte solution. The electrolyte solutions consisted of NaCl solutions of 0.01, 0.1 and 1 mol dm^{-3} concentrations. The bubbles were visualized at 1000 photographs per second using the 512 × 512 pixel SR-CMOS imaging sensor array at a magnification of 400×.

3. Results and discussion

3.1. Generation of hydrogen bubbles

In a previous investigation, the flowing water was electrolyzed using an SPE electrolyzer. On the cathode side of the SPE electrolyzer, hydrogen was generated and dissolved into the flowing water [24]. The hydrogen was generated between the plated Pt electrode and the Nafion. The hydrogen was then released through the electrode crack forming bubbles in the water on the outer side of the plated Pt electrode. A quantity of the generated hydrogen is known to have penetrated into the Nafion [27]. In the present investigation, the generated bubble was captured by an X-ray imaging camera [28,29]. Phase-contrast X-ray imaging is a convenient means to visualize the bubble shape in terms of the large density difference at the gas–liquid interface. Additionally, X-rays can pass through the thin plated Pt electrode. Using a single-sided Pt electrode, two kinds of hydrogen bubbles are simultaneously captured by the X-ray imaging camera. These two types of bubbles include the hydrogen bubble that adheres to the Pt electrode released through the crack of the electrode, and the hydrogen bubble that adheres to the Nafion membrane and is released through the Nafion.

Fig. 4 shows the time dependence of the hydrogen bubble's diameter under 20 mA electrolysis in filled chamber II. Two types of bubbles were measured under these conditions. One was a slowly growing bubble that takes 150 s to grow 500 μm in diameter. The calculated volume velocity of the bubble generation was 4.9×10^{-7} cm^3 s^{-1}. The other was a quickly growing bubble that took 25 s to grow 500 μm in diameter. The calculated volume velocity of bubble generation was 4.0×10^{-6} cm^3 s^{-1}. In an empty chamber II, the quickly growing bubble was not measured. The quickly growing bubble was determined to adhere to the Pt electrode, while the slowly growing bubble adhered to the Nafion. The volume velocity of the bubbles passing through the Nafion was one-tenth as large as that passing through the Pt crack. In the previous investigation, the sum of the mole quantities of dissolved hydrogen and gaseous hydrogen was not equal to the mole quantity calculated from the current. For the most part, the lost mole quantity calculated from the current was the mole quantity of the hydrogen that passed through the Nafion.

In the case in which the anode electrode was plated opposite the cathode, the oxygen was generated between the Pt anode and the Nafion, and the oxygen was determined to pass through the Nafion as well. The pressure in the SPE is thought to be increased, and the ratio of the hydrogen volume passing through the electrode crack will increase.

3.2. Contraction of hydrogen bubbles

The hydrogen bubble that adhered to the Pt was captured using an X-ray imaging camera. Fig. 5 shows the time dependencies of the hydrogen bubble's diameter after turning off the current. The slowly contracting bubble adhered to a single-sided Pt plated Nafion, and was observed to disappear in 500 s. The calculated volume velocity of the bubble contraction was 5.6×10^{-8} cm^3 s^{-1}. In contrast, the quickly contracting bubble adhered to double-sided Pt plated Nafion and took only 60 s to disappear. The calculated volume velocity of bubble contraction was 2.2×10^{-7} cm^3 s^{-1}. The two bubbles were approximately the same magnitude when they were first generated. Using a double-sided Pt electrode plated to Nafion, oxygen was generated between the anode and the Nafion. Further, hydrogen was generated between the cathode and the Nafion. After turning off the current, the generated hydrogen and oxygen passed through the Nafion from both sides to the opposing Pt electrode. Hydrogen reacted with oxygen, forming water. In water electrolysis using an SPE electrolyzer, the amount of gas that permeates into Nafion is a small. However, this is considered a significant minority, since it is the loss of electrolysis.

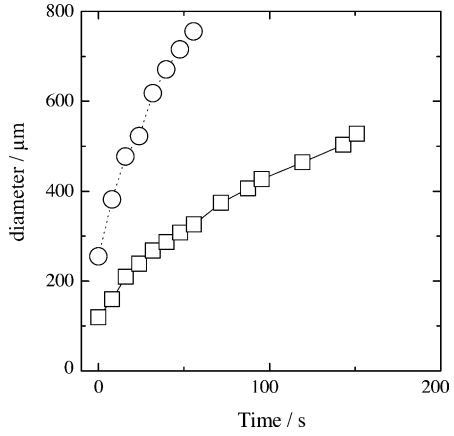

Fig. 4. Time dependency of bubble diameter adhering to Pt electrode (◯) or Nafion (□).

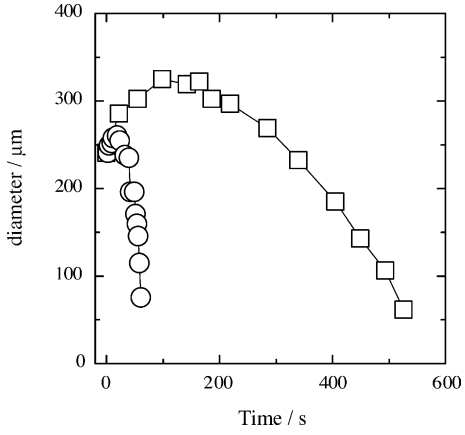

Fig. 5. Time dependency of bubble diameter adhering to a single-sided Pt plated (□) or double-sided Pt plated (◯).

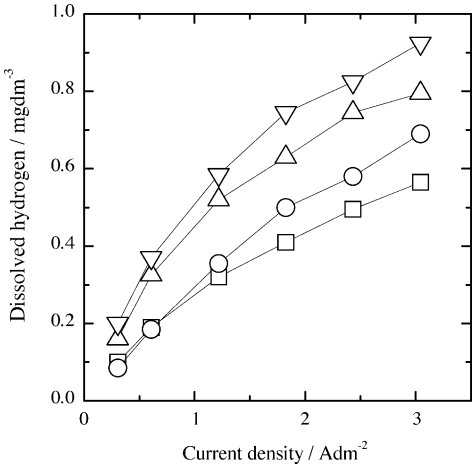

Fig. 6. Concentration changes of dissolved hydrogen with current density at different concentrations of electrolytes. (□) Distilled water; NaCl solutions of: (◯) 0.01 mol dm^{-3}, (△) 0.1 mol dm^{-3} and (▽) 1 mol dm^{-3} concentrations.

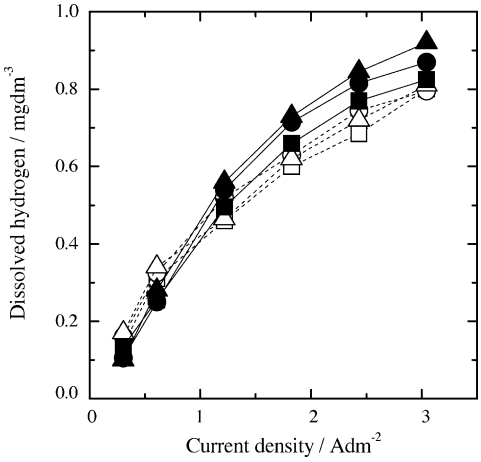

Fig. 7. Concentration changes of dissolved hydrogen with current density at different electrolyte solutions. Electrolyte solution consisted of 0.1 mol dm^{-3} of: (■) LiCl; (●) NaCl; (▲) KCl; (□) Li_2SO_4; (◯) Na_2SO_4; (△) K_2SO_4.

3.3. Effect of electrolyte

3.3.1. Concentration dependence

The electrolysis cell in Fig. 3 was used to clarify the electrolyte effect on the concentration of dissolved hydrogen. Dissolved hydrogen is dissolved into water as H_2 molecule. Fig. 6 shows the hydrogen concentration in electrolyzed water as a function of the current density in distilled water and NaCl solution of differing concentrations. The concentration of dissolved hydrogen was observed to increase with current density in both solutions. At a low current density, there was not much of a difference in the concentration of dissolved hydrogen, regardless of the concentration of the electrolyte. At high current density, however, the greatest amount of hydrogen dissolved in the electrolyzed water was observed at the electrolyte highest concentration. The same observation was made for the KCl, LiCl, Na_2SO_4, K_2SO_4 and Li_2SO_4 solutions of differing concentrations.

3.3.2. Effect of ionic species

Fig. 7 shows the dissolved hydrogen concentration in electrolyzed water as a function of the current in different kinds of cationic species solutions of 0.1 mol dm^{-3}. The cationic species had no obvious effect on the concentration of dissolved hydrogen. The concentration of dissolved hydrogen was less in the presence of Li^+ than Na^+ or K^+, at every concentration of electrolyte solution. Further, the dissolved hydrogen increased slightly with Li^+, Na^+ and K^+, corresponding to the increase in the Stokes' radius. However, these differences were very difficult to distinguish.

3.3.3. Relation of ionic strength

Fig. 8 shows the dissolved hydrogen concentration in electrolyzed water as a function of the ionic strength at different current densities. The concentration of dissolved hydrogen increased with the logarithm of ionic strength, independent of the ionic species. At low current density, the concentration was not concerned with ionic strength.

3.4. Coalescence of hydrogen bubbles

The floating bubbles were captured on the film using a high speed digital imaging camera on the upper, middle and lower sides of the SPE electrode. Fig. 9 shows the bubble motion on the lower side of the SPE electrode, in distilled water. The images shown in Fig. 9 were taken every 5 ms. The large bubbles rose faster than the small bubbles. The rising large bubbles incorporate the small bubbles, thereby increasing their size.

Fig. 10 shows the bubble motion on the lower side of the SPE electrode, in a 1 mol dm^{-3} NaCl solution. The images in Fig. 10 were taken every 5 ms. The small bubble in a 1 mol dm^{-3} NaCl solution was not incorporated by larger

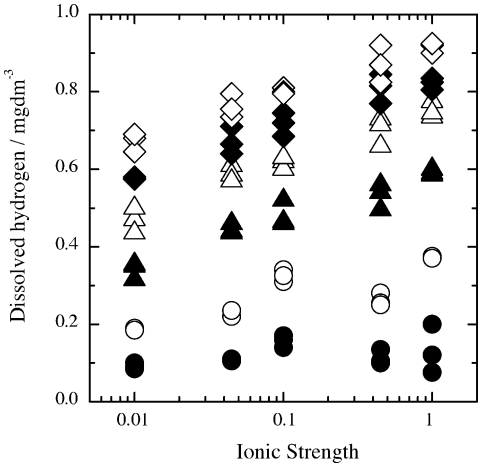

Fig. 8. Relationship between ionic strength and concentration of dissolved hydrogen. Current density: (●) 0.3 A dm^{-2}; (◯) 0.6 A dm^{-2}; (▲) 1.2 A dm^{-2}; (△) 1.8 A dm^{-2}; (♦) 2.4 A dm^{-2}; (◇) 3.0 A dm^{-2}.

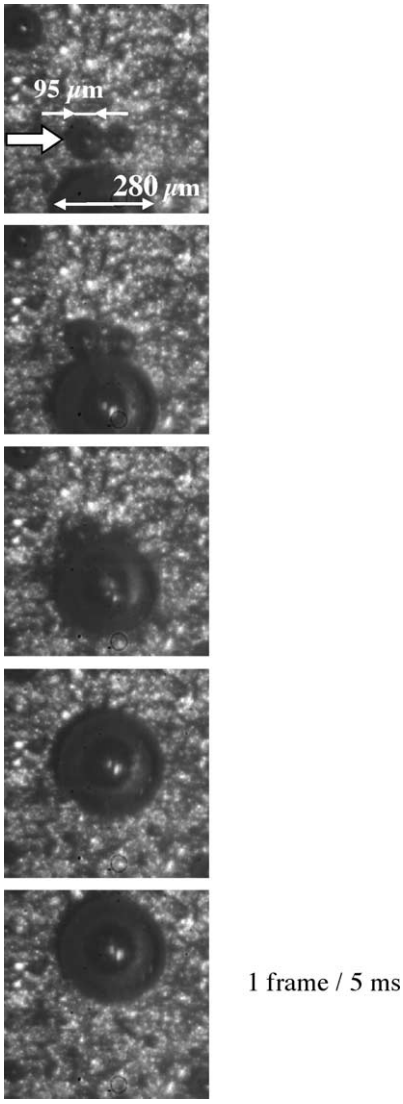

Fig. 9. Photographic sequence of floating bubbles in distilled water (1 photograph/5 ms). The small bubble is indicated with an arrow.

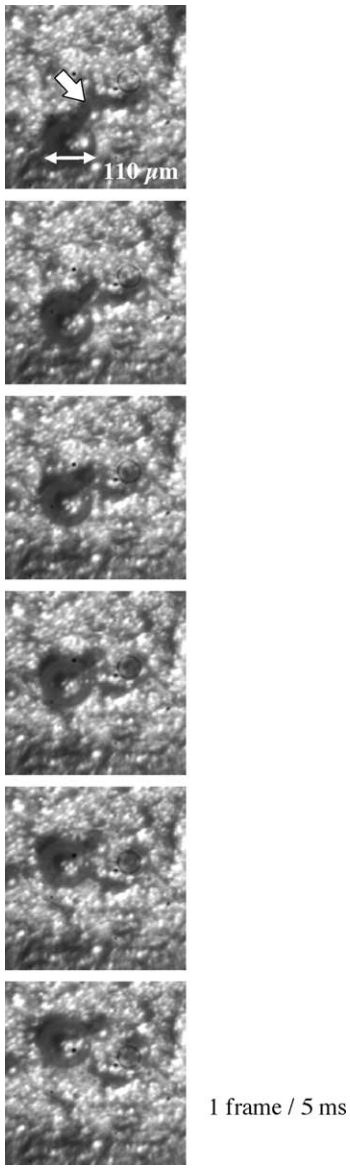

Fig. 10. Photographic sequence of floating bubbles in a 1 mol dm^{-3} NaCl solution (1 photograph/5 ms). The small bubble is indicated with arrow.

bubbles; it was repelled by the large bubbles. A number of researchers have observed that bubble coalescence is inhibited by electrolytes. The hydrogen bubble was released from the crack of the plated electrode into the water using an SPE electrolyzer [25]. The amount of the dissolved hydrogen from the bubble was dependent on the bubble size, since the inner pressure and the rising velocity were greatly affected by the bubble size. At high electrolyte concentrations, the bubbles do not readily coalesce into a large bubble. The bubble in the bulk water can maintain the size of the released bubble under high current density. Thus, the high concentration of the dissolved hydrogen was attributed to inhibition of the bubble coalescence by the electrolyte.

3.4.1. Distribution of bubble diameters

The bubble diameter was measured at the upper, middle and lower sides of the SPE electrode. Fig. 11 shows the distribution of bubble diameters in distilled water and Fig. 12 shows it in a 1 mol dm^{-3} NaCl solution. In distilled water, the percentage of bubbles with a diameter less than 100 μm was about 70% on the lower side of the SPE electrode, and a large percentage of the bubble diameters were less than 400 μm. On the upper side, the percentage of bubbles with diameters less than 100 μm was about 40% and bubbles with diameters larger 400 μm were visible. In contrast, in a 1 mol dm^{-3} NaCl solution, the percentage of bubbles with diameters less than 100 μm was about 80% on all three sides of the SPE electrode, and the bubbles with diameters of more than 400 μm were not visible. Fig. 13 shows the distribution of bubble diameters on the upper side of the SPE electrode in the distilled water and NaCl solutions. In a 0.01 and 0.1 mol dm^{-3} NaCl solution, the percentage of bubbles whose diameter was less than 100 μm was 40 and 70%, respectively. Furthermore,

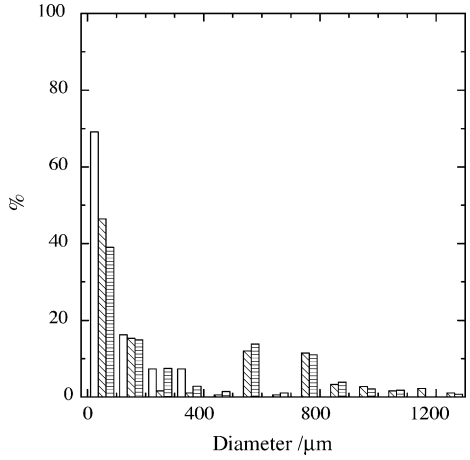

Fig. 11. Distribution of bubble diameter in the distilled water visualized at the upper (▤), middle (▧) and lower sides (□) of the electrode.

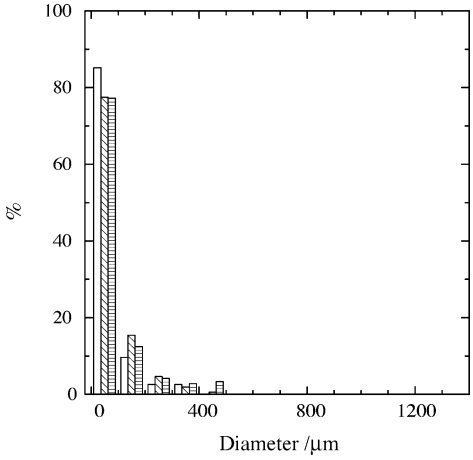

Fig. 12. Distribution of bubble diameter in 1 mol dm^{-3} NaCl solution visualized at upper (▤), middle (▧) and lower sides (□) of the electrode.

in a 0.01 mol dm^{-3} NaCl solution, the percentage of bubbles with a diameter ranging from 100 to 200 μm was significantly higher than in distilled water. It is known that the higher the electrolyte concentration, the lower the probability of bubble coalescence. The rise velocity of the small bubble was

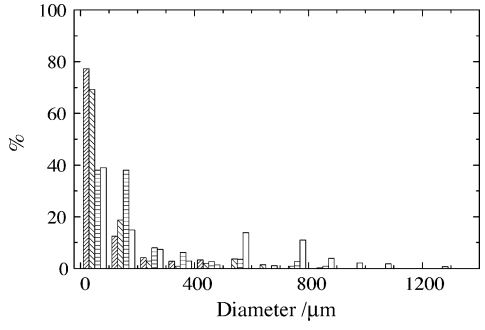

Fig. 13. Distribution of bubble diameter at the upper side of the electrode. Concentration of NaCl solution: 0 mol dm^{-3} (□); 0.01 mol dm^{-3} (▤); 0.1 mol dm^{-3} (▧); 1 mol dm^{-3} (▨).

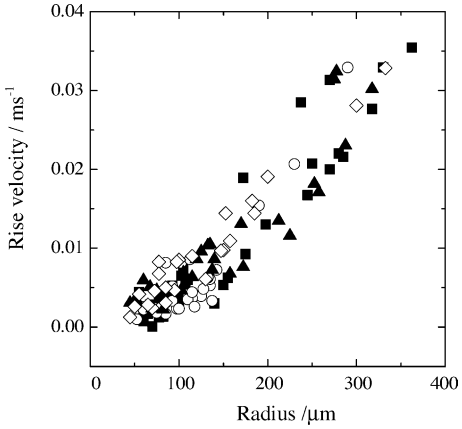

Fig. 14. Rise velocity of bubble with bubble diameter at different concentrations of NaCl solutions. Concentration of NaCl solution: 0 mol dm^{-3} (■); 0.01 mol dm^{-3} (◯); 0.1 mol dm^{-3} (▲); 1 mol dm^{-3} (◊).

observed to be slower than that of the large bubble. Additionally, the inner pressure of a small bubble is higher than that of a large bubble. As a result, the higher the electrolyte concentration, the more the hydrogen dissolves.

3.4.2. *Bubble rise velocity*

Fig. 14 shows the bubble rise velocity as a function of the diameter at various electrolyte concentrations. It was found that the larger the diameter of the bubble, the faster the rise velocity. It is obvious that the coalesced large bubble rises much faster than the non-coalesced small bubbles.

Kellermann et al. reported that the bubble rise velocity in electrolyte solutions depended strongly on the electrolyte concentration [22]. However, in this work, the distribution of bubble rise velocity was too large. A correlation between the bubble rise velocity and dependence on the electrolyte concentration was not observed. Kellermann measured the rise velocity with a single bubble that rises in the water, but under the current SPE electrolysis conditions, the motion of other bubbles affect bubble rise velocity.

Thus, it appears that the velocity dependency on electrolyte concentration was smaller than that on diameter.

4. Conclusions

In a single-sided plated SPE electrolyzer, the hydrogen bubbles adhering to both sides of the Nafion–Pt complex electrode were simultaneously captured by X-ray contrast imaging. The calculated volume velocity of bubbles passing through the Nafion was one-tenth as large as that passed through the Pt crack.

On the double-sided plated SPE electrolyzer, electrolysis was performed in electrolyte solutions at different concentrations. The concentration of dissolved hydrogen was sensitive to the electrolyte concentration. As the electrolyte concentration increased, the hydrogen was further dissolved. It is important to note that hydrogen dissolved more at a high

current density. Hydrogen bubbles were visualized using a high speed camera. It was clear that the degree of bubble coalescence was high in the distilled water, but that the bubble coalescence was inhibited by the electrolyte. The hydration forces were reported to inhibit bubble coalescence [19,30]. This hydration force was caused by the need to expel water molecules from the film between the bubbles. Addition of electrolytes increases the repulsive hydration forces by enhancing the water structure due to hydrogen bonds. If coalescence does not occur, the released bubble maintains a small diameter. The small bubble is readily dissolved into water creating a high inner pressure. A high concentration of dissolved hydrogen is attributable to the bubble coalescence being inhibited by the electrolyte.

Acknowledgement

The synchrotron radiation experiments were performed in BL19B2 of SPring-8 with the approval of the Japan Synchrotron Radiation Research Institute (JASRI) (Proposal No. 2003B0239-NI-np).

References

[1] H. Tashiro, T. Kitahora, K. Sumiyoshi, Y. Fujiyama, T. Bamba, 2nd Function Water Symposium'95, Kyoto, 1995, p. 20.
[2] Y. Naito, T. Takagi, K. Uchiyama, N. Tomatsuri, K. Matsuyama, T. Fujii, N. Yagi, N. Yoshida, T. Yoshikawa, J. Clin. Biochem. Nutr. 32 (2002) 69.
[3] S. Shirahata, S. Kabayama, M. Nakano, T. Miura, K. Kusumoto, M. Gotoh, H. Hayashi, K. Otsubo, S. Morisawa, Y. Katakura, Biochem. Biophys. Res. Commun. 234 (1997) 269.
[4] S. Shibata, Bull. Chem. Soc. Jpn. 36 (1963) 53.
[5] K. Kikuchi, H. Takeda, B. Rabolt, T. Okaya, Z. Ogumi, Y. Saihara, H. Noguchi, J. Appl. Electrochem. 31 (2001) 1301.
[6] K. Kikuchi, H. Takeda, B. Rabolt, T. Okaya, Z. Ogumi, Y. Saihara, H. Noguchi, J. Electroanal. Chem. 506 (2001) 22.
[7] L.J. Nuttall, Proceedings of 16th Intersociety Energy Conversion Engineering Conference, vol. 2, 1981, p. 1425.
[8] H. Takenaka, E. Torikai, Y. Kawami, N. Wakabayashi, T. Sakai, Denki Kagaku 53 (1985) 261.
[9] Y. Fukui, S. Yuu, AIChE J. 28 (1982) 866.
[10] A. Graciaa, G. Morel, P. Saulner, J. Lachaise, R.S. Schechter, J. Colloid Interface Sci. 172 (1995) 131.
[11] R.H. Yoon, J.L. Yordan, J. Colloid Interface Sci. 113 (1986) 430.
[12] G.L. Collins, M. Motarjemi, G.J. Jameson, J. Colloid Interface Sci. 63 (1978) 69.
[13] N.P. Brandon, G.H. Kelsall, S. Levine, A.L. Smith, J. Appl. Electrochem. 15 (1985) 485.
[14] C. Yang, T. Dabros, D. Li, J. Czarnecki, J.H. Masliyah, J. Colloid Interface Sci. 243 (2001) 128.
[15] M.A. Zarra, Chem. Biochem. Eng. Q. 13 (1999) 47.
[16] V.S.J. Craig, B.W. Ninham, R.M. Pashley, Nat. Lett. 364 (1993) 317.
[17] M.E. Aguilera, A. Ojeda, C. Rondon, A.L. Ramos, Ann. N. Y. Acad. Sci. 972 (2002) 242.
[18] G.H. Kelsall, S. Tang, S. Yurdakul, A.L. Smith, J. Chem. Soc., Faraday Trans. 92 (1996) 3887.
[19] Y.H. Tsang, Y.H. Koh, D.L. Koch, J. Colloid Interface Sci. 275 (2004) 290.
[20] P. Boissonneau, P. Byrne, J. Appl. Electrochem. 30 (2000) 767.
[21] N.K. Khosla, S. Venkatachalam, P. Somasundaran, J. Appl. Electrochem. 21 (1991) 986.
[22] H. Kellermann, K. Juttner, G. Kreysa, J. Appl. Electrochem. 28 (1998) 311.
[23] W. James, G. Tyrrell, P. Attard, Phys. Rev. Lett. 87 (2001) 176104.
[24] J.Y. Kim, M.G. Song, J.D. Kim, J. Colloid Interface Sci. 223 (2000) 285.
[25] Y. Tanaka, S. Uchinashi, Y. Saihara, K. Kikuchi, T. Okaya, Z. Ogumi, Electrochim. Acta 48 (2003) 4013.
[26] Y. Tanaka, K. Kikuchi, Y. Saihara, Z. Ogumi, Electrochim. Acta 50 (2005) 5229.
[27] Z. Ogumi, Z. Takehara, S. Yoshizawa, J. Electrochem. Soc. 131 (1984) 769.
[28] H. Takano, Y. Suzuki, K. Uesugi, A. Takeuchi, N. Yagi, Proc. SPIE 4499 (2001) 126.
[29] Y. Kagoshima, Y. Tsusaka, K. Yokoyama, K. Takai, S. Takeda, J. Matsui, Jpn. J. Appl. Phys. Part 2 38 (1999) L470.
[30] V.S.J. Craig, B.W. Ninham, R.M. Pashley, J. Phys. Chem. 97 (1993) 10192.